PHYSICAL REVIEW C **96**, 064001 (2017)

Complete set of deuteron analyzing powers from $\vec{d}p$ elastic scattering at 190 MeV/nucleon

K. Sekiguchi,[1,*] H. Witała,[2] T. Akieda,[1] D. Eto,[1] H. Kon,[1] Y. Wada,[1] A. Watanabe,[1] S. Chebotaryov,[3] M. Dozono,[4] J. Golak,[2] H. Kamada,[5] S. Kawakami,[6] Y. Kubota,[4] Y. Maeda,[6] K. Miki,[1] E. Milman,[3] A. Ohkura,[7] H. Sakai,[8] S. Sakaguchi,[7] N. Sakamoto,[8] M. Sasano,[8] Y. Shindo,[7] R. Skibiński,[2] H. Suzuki,[8] M. Tabata,[7] T. Uesaka,[8] T. Wakasa,[7] K. Yako,[4] T. Yamamoto,[6] Y. Yanagisawa,[8] and J. Yasuda[7]

[1]*Department of Physics, Tohoku University, Sendai, 980-8578, Japan*
[2]*M. Smoluchowski Institute of Physics, Jagiellonian University, PL-30-348 Cracow, Poland*
[3]*Department of Physics, Kyungpook National University, Daegu 702-701, Korea*
[4]*Center for Nuclear Study, University of Tokyo, Tokyo, 113-0033, Japan*
[5]*Department of Physics, Kyushu Institute of Technology, Kitakyushu 804-8550, Japan*
[6]*Faculty of Engineering, University of Miyazaki, Miyazaki, 889-2192, Japan*
[7]*Department of Physics, Kyushu University, Fukuoka, 819-0395, Japan*
[8]*RIKEN Nishina Center, Wako, 351-0198, Japan*

(Received 12 July 2017; revised manuscript received 29 October 2017; published 6 December 2017)

All deuteron analyzing powers for elastic deuteron-proton (dp) scattering have been measured with a polarized deuteron beam at 186.6 MeV/nucleon. They are compared with results of three-nucleon Faddeev calculations based on the standard, high-precision nucleon-nucleon (NN) potentials alone or combined with commonly used three-nucleon force (3NF) models such as the Tucson-Melbourne '99 or the Urbana IX. Predicted 3NF effects localized at backward angles are supported only partially by the data. The data are also compared to predictions based on locally regularized chiral NN potentials. An estimation of theoretical truncation uncertainties in the consecutive orders of chiral expansion suggests that the observed discrepancies between this modern theory and the data could probably be explained by including chiral 3NF's in future calculations. A systematic comparison to the deuteron analyzing power data previously taken at incident energies from 70 to 294 MeV/nucleon clearly shows that not only the cross section but also the analyzing powers reveal growing 3NF effects when the three-nucleon system energy is increased.

DOI: 10.1103/PhysRevC.96.064001

I. INTRODUCTION

One of the main interests of nuclear physics is to understand the forces acting between nuclear constituents. Recently, the importance of the three-nucleon force (3NF) in the nuclear Hamiltonian has been studied in few-nucleon systems as well as in many-nucleon systems [1–3]. Three-nucleon (3N) systems, where numerically exact solutions of the corresponding Faddeev equations for any two- and three-nucleon forces are feasible, play an especially important role in these investigations.

Nucleon-deuteron (Nd) scattering offers a good opportunity to study dynamical aspects of 3NFs, which are momentum, spin, and isospin dependent, since it provides not only cross sections but also a variety of spin observables at different incident nucleon energies. The past two decades have witnessed extensive experimental and theoretical investigations of the Nd scattering performed in a wide range of incoming nucleon energies up to $E \sim 300$ MeV/nucleon (MeV/N). Theoretical progress has made it possible to perform rigorous numerical Faddeev calculations of the 3N scattering using semiphenomenological NN interactions such as the AV18 [4], CDBonn [5], and Nijmegen 1 and 2 [6] potentials, which describe existing two-nucleon (2N) data with very high precision up to 350 MeV. Incorporating in these calculations the 2π-exchange 3NF models such as the Tucson-Melbourne '99 (TM99) [7] or Urbana IX [8] have provided clear indications that the 3NFs play an important role in the 3N Hamiltonian [9–12]. Experimentally, developments in the technology of highly polarized proton and deuteron ion sources, their application in recently constructed accelerators, sophisticated techniques of target polarization, and construction of high-precision polarimeters have made it possible to get precise data not only for the cross section but also for the spin observables up to $E \sim 300$ MeV/N [13–33]. The experimental success in obtaining high-precision data for the Nd scattering together with theoretical achievements have made this process a solid testing ground for modern nuclear forces.

The evidence for strong 3NF effects in Nd scattering came first from a study of the neutron-deuteron (nd) total cross section [10,11] and elastic scattering angular distribution [9]. Starting at incoming nucleon energies above ≈60 MeV, theoretical predictions obtained with NN potentials tend to clearly underestimate the data. The deviation between data and the predictions based on the NN forces grows rapidly with the incident energy. Including the TM99 or the Urbana IX 3NF's, with parameters adjusted to reproduce the ^{3}H and ^{3}He binding energies, allows one to achieve agreement between theory and data for both Nd elastic scattering and the nd total cross sections up to ≈130 MeV. However, contrary to the results obtained at these lower energies, for higher incident energies the discrepancies between the data and the calculations are only partially reduced, even when

*kimiko@lambda.phys.tohoku.ac.jp

including the 3*N*Fs. In order to exclude the possibility that relativistic effects could be responsible for those higher energy discrepancies, the nonrelativistic 3*N* Faddeev equations were reformulated to include basic relativistic features such as the proper relativistic energy-momentum relation, relativistic *NN* interactions with their proper boosts, and Wigner spin rotations [34,35]. It turned out that effects of relativity are practically negligible for the elastic scattering differential cross section and spin observables as well as for the total *nd* cross section. Thus, the higher energy discrepancies between theory and data must result from short-range 3*N*F components, which become active at higher energies.

Also, for spin observables in elastic *Nd* scattering, a complex pattern of discrepancies between theory and data has been found. For some spin observables, the effects of 3*N*F's depend on whether the AV18 *NN* potential is combined with the TM99 or the Urbana IX 3NF interaction [12]. It may indicate possible inconsistencies between *NN* potentials and 3*N*F models commonly used in 3*N* calculations.

These inconsistencies can be cured in the chiral effective field theory (EFT) approach, which allows one to derive consistent nuclear forces acting in many-nucleon systems. It provides consistent *NN* and 3*N* forces in a systematically improvable way: order by order in chiral expansion, starting from the leading order (LO). Accurate *NN* potentials at N^3LO have been available for about a decade [36,37] and 3*N*F's, starting at N^2LO [38], have been derived up to N^3LO [39,40]. Recently, the *NN* potentials up to the fifth order (N^4LO) in the chiral expansion, based on the improved regularization framework, have been presented [41,42]. These chiral *NN* potentials offer an excellent description of the *NN* data and provide a solid basis for few-body calculations.

In this paper, we present a complete set of deuteron analyzing powers for elastic deuteron-proton (*dp*) scattering newly obtained with the 186.6 MeV/nucleon (MeV/*N*) polarized deuteron beam at the RIKEN RI Beam Factory (RIBF). This measurement is a part of the systematic studies of the deuteron analyzing powers for elastic *dp* scattering at 70–294 MeV/*N* at the RIBF [13,16,18,33,43]. In order to clarify the energy dependence, the deuteron analyzing powers at 70 and 135 MeV/*N* previously obtained by us are also shown in the present paper. We compare the data to the theoretical predictions based on the standard *NN* potentials, namely the CD Bonn, AV18, and Nijmegen 1 and 2, alone or combined with the commonly used 3*N*F models, the TM99 and Urbana IX. In addition to these spin observables, we compare theoretical calculations to *Nd* elastic scattering cross-section data measured previously at 70, 135, and 190 MeV/*N* by us and the others. To reveal similarities and to find differences between the standard and chiral *NN* potentials, we compare previously mentioned predictions with the results based on the improved, locally regularized N^4LO*NN* potential of Refs. [41,42]. The availability of these theoretical predictions in successive orders of chiral expansion up to N^4LO allows us to calculate theoretical uncertainties for each observable due to a truncation to a particular order of chiral expansion. Based on that, we can indicate the order of chiral expansion required to interpret the *Nd* scattering data with sufficient precision.

In Sec. II, we describe the experimental procedure and the data analysis. A brief description of the theoretical formalism and forces used in the calculations is given in Sec. III. In Sec. IV, the theoretical predictions are compared with the data. Finally, in Sec. V, we summarize and conclude.

II. EXPERIMENTAL PROCEDURE AND DATA ANALYSIS

A measurement of a complete set of the deuteron analyzing powers for elastic *dp* scattering at the deuteron laboratory energy of 373.2 MeV (186.6 MeV/*N*) was performed with the BigDpol system at the RIBF. Only the main features of the experimental procedure and data analysis are briefly summarized in the following; the detailed description can be found in Refs. [33,43].

The vector and tensor polarized deuteron beams provided by the polarized ion source [44] were first accelerated by the azimuthally varying field (AVF) and Ring cyclotrons up to 70 MeV/*N*, and then up to 186.6 MeV/*N* by the superconducting cyclotron SRC. The BigDpol, located at the extraction beam line of the SRC, consisted of the target chamber, aluminum cone window, and detector holders. The deuteron beams of intensities of 4–8 nA bombarded a polyethylene (CH_2) target with a thickness of 330 mg/cm^2, placed in the scattering chamber. The four pairs of plastic scintillation counters coupled with photomultiplier tubes were mounted in two independent planes perpendicular to each other. The opening angle of the BigDpol was $7-70^\circ$ in the laboratory system. The scattered deuterons and recoil protons were detected under a kinematical coincidence condition by each pair of the detectors, which was essential to discriminate the elastic *dp* scattering events from events produced by other scattering processes. The solid angles were determined by the proton detectors with the angular range $\Delta\theta_{\text{laboratory.}} = \pm 1^\circ$. The deuteron beam was stopped in a Faraday cup placed at the focal plane F0 of the BigRIPS spectrometer [45].

The data were taken with polarized and unpolarized beams and the following pairs of the vector, p_Z, and tensor, p_{ZZ}, polarizations were applied (in terms of the theoretical maximum values): $(p_Z, p_{ZZ}) = (0,0)$, $(1/3,-1)$, $(-2/3,0)$, and $(1/3,1)$. The polarizations were changed cyclically at intervals of 5 s by switching the radio frequency (RF) transition units of the polarized ion source. The beam polarizations were monitored continuously with the beam line polarimeter Dpol using elastic *dp* scattering at 70 MeV/*N* [46]. At the RIBF, the single-turn extractions were available for all the cyclotrons used. Therefore, depolarizations were expected to be small during beam acceleration. In the present measurement, the beam polarizations achieved 60–70% of the theoretical maximum values.

The analyzing powers iT_{11}, T_{20}, and T_{22} were measured simultaneously with the deuteron spin normal to the horizontal plane. For the T_{21} measurement, the spin symmetry axis was rotated in the horizontal plane and aligned at an angle $\beta = 45.0^\circ \pm 1.1^\circ$ with respect to the beam direction. In this experiment, the polarization axis of the deuteron beam was rotated with a Wien filter system prior to acceleration [47].

An identification of the scattered deuterons and recoil protons for *dp* elastic scattering events was performed by using the light outputs in the scintillation detectors. Accidental coincidences were estimated by coincidence triggering between adjacent beam bunches. After subtracting accidental coincidences, peaks from dp elastic scattering were clearly identified both for the deuteron and proton detectors. The effects of the backgrounds other than accidental coincidences, for example, events due to the proton knock-out reaction and those from the deuteron breakup reaction, were estimated by changing the integration range of a peak of elastic dp scattering for the deuteron and proton detectors, respectively. The results for the analyzing powers changed by 0.005 or less.

The experimental results for the deuteron analyzing powers are shown as (black) circles in the panels (e) and (f) of Figs. 1–4 and are listed in Table I. In the figures, only statistical uncertainties are shown. Their values are less than 0.02, 0.02, 0.02, and 0.01 for iT_{11}, T_{20}, T_{21}, and T_{22}, respectively. The uncertainty of the deuteron beam polarization is less than 4%. The uncertainties from the background events do not override the statistical ones.

III. THEORETICAL FORMALISM AND DYNAMICAL INPUTS

Nd scattering with nucleons interacting through a NN potential and through a $3N$F is described in terms of a $3N$ scattering operator T which satisfies the Faddeev-type integral equation [1,48,49]. We refer to Refs. [1,49,50] for a general overview of $3N$ scattering and for details on the practical implementation of the Faddeev equations.

We solved the $3N$ Faddeev equation in a partial wave momentum-space basis for three values of the incoming nucleon laboratory energy $E = 70, 135,$ and 190 MeV. As an NN interaction, we used the high-precision semiphenomenological AV18, CD Bonn, and Nijmegen 1 and 2 potentials. We took these interactions alone or together with the TM99 $3N$F. In the latter case, for each NN potential separately, the Λ cutoff parameter of the TM99 $3N$ force was adjusted so that this particular combination of an NN and $3N$ force reproduced the experimental triton binding energy [12]. The AV18 potential was also combined with the Urbana IX $3N$F. All these combinations allowed us to find not only the magnitude of $3N$F effects but also their dependence on a specific model of the nuclear interactions.

We solved the 3N Faddeev equation also with the locally regularized chiral NN interactions of Refs. [41,42]. These new NN chiral forces were constructed up to N^{4}LO order of chiral expansion and employ a regularization scheme in the coordinate space using the local regulator $f(r) = [1 - \exp(-r^2/R^2)]^6$ with the regulator parameter $R =$ 0.8,0.9,1.0,1.1, and 1.2 fm. Such a regularization led, in particular, to a significant reduction of finite-cutoff artifacts [41,42,51] observed for the older versions of the chiral potentials [36,37]. In the present calculations, we used the regulator $R = 0.9$ fm, which yields the best description of the NN data. Solutions of the 3N Faddeev equation for the consecutive orders, from LO to N^{4}LO, allowed us to estimate the theoretical uncertainty for various observables calculated at different chiral orders bound with a truncation of chiral expansion to a particular order, according to procedure described in Ref. [52].

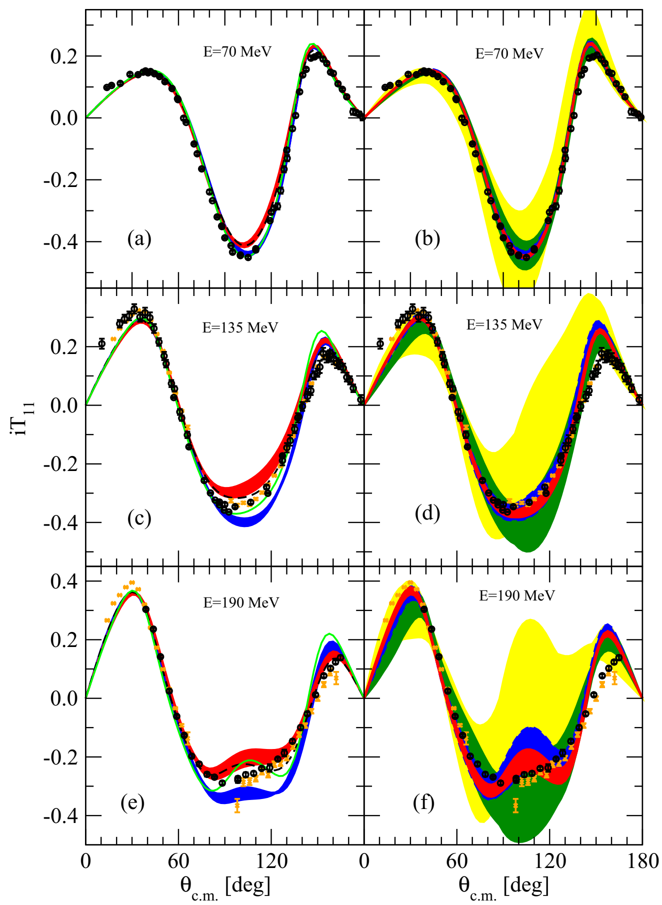

FIG. 1. The elastic Nd scattering deuteron vector analyzing power iT_{11} at the incoming nucleon laboratory energies $E = 70$ MeV [(a), (b)], 135 MeV [(c), (d)], and 190 MeV [(e), (f)]. In panels (a), (c), and (e), the dark shaded (blue) band covers predictions of standard NN potentials (the AV18, CD Bonn, and Nijmegen 1 and 2 alone) and the light shaded (red) band shows predictions when they are combined with the TM99 $3N$F. The dashed (black) curve represents the prediction of the AV18 + Urbana IX combination. The solid (green) curve shows prediction of the locally regularized (regulator $R = 0.9$ fm) N^{4}LO chiral potential. In panels (b), (d), and (f), the estimated theoretical uncertainties at different order of chiral expansion are shown by the bands of increasing width at N^{4}LO (red), N^{3}LO (blue), N^{2}LO (green), and NLO (yellow). The (black) circles are dp data: in panels (a) and (b) from Refs. [18,46], in panels (c) and (d) from Refs. [13,16,18,46], and in panels (e) and (f) from our new dp data. The (orange) x symbols are pd data: at 135 MeV in panels (c) and (d) and at 200 MeV in panels (e) and (f) from Ref. [26].

When solving the $3N$ Faddeev equation we included all $3N$ partial wave states with total two-nucleon angular momentum $j \leqslant 5$ and total $3N$ angular momentum $J \leqslant 25/2$.

IV. COMPARISON OF DATA WITH THEORETICAL PREDICTIONS

We show our new data set of the deuteron analyzing powers at 186.6 MeV/N in the panels (e) and (f) of Figs. 1–4 as (black) circles. In these figures, also the deuteron analyzing powers taken at 200 MeV/N from Ref. [26] are shown by (orange)

TABLE I. Data table for all deuteron analyzing powers in *dp* elastic scattering at the deuteron laboratory energy of 373.2 MeV (186.6 MeV/nucleon) together with the statistical uncertainties.

$\theta_{\mathrm{c.m.}}$(deg)	iT_{11}	ΔiT_{11}	T_{20}	ΔT_{20}	T_{21}	ΔT_{21}	T_{22}	ΔT_{22}
38.9	0.304	0.004	0.024	0.008		c	−0.181	0.003
43.7	0.236	0.004	0.029	0.009	−0.032	0.007	−0.211	0.004
48.4	0.142	0.004	0.062	0.010			−0.250	0.004
54.1	0.025	0.004	0.090	0.011	−0.045	0.004	−0.274	0.004
58.9	−0.061	0.004	0.121	0.014			−0.302	0.006
63.7	−0.127	0.004	0.137	0.012	−0.114	0.004	−0.324	0.005
68.6	−0.197	0.005	0.151	0.016	−0.159	0.007	−0.335	0.006
73.4	−0.224	0.006	0.109	0.023	−0.198	0.005	−0.331	0.009
78.4	−0.260	0.007	0.104	0.015	−0.232	0.007	−0.335	0.006
83.3	−0.269	0.003	0.083	0.015			−0.309	0.006
88.3	−0.289	0.006	0.055	0.013	−0.283	0.007	−0.284	0.005
98.4	−0.274	0.007	−0.008	0.013	−0.282	0.004	−0.226	0.005
103.5	−0.260	0.008	−0.015	0.014	−0.270	0.011	−0.197	0.006
108.6	−0.256	0.006	−0.020	0.012	−0.245	0.006	−0.172	0.005
113.8	−0.239	0.005	0.035	0.009	−0.231	0.008	−0.163	0.004
119.0	−0.238	0.013	0.025	0.017	−0.250	0.011	−0.146	0.007
124.2	−0.207	0.004	−0.013	0.008	−0.285	0.007	−0.142	0.003
128.4	−0.187	0.012	−0.054	0.019	−0.310	0.007	−0.148	0.008
133.7	−0.146	0.006	−0.122	0.012	−0.348	0.007	−0.146	0.005
139.0	−0.099	0.006	−0.179	0.012	−0.373	0.007	−0.149	0.005
143.3	−0.053	0.006	−0.216	0.012	−0.420	0.009	−0.152	0.005
148.6	0.012	0.006	−0.277	0.011	−0.446	0.008	−0.171	0.004
154.0	0.077	0.006	−0.330	0.012	−0.484	0.011	−0.178	0.005
158.3	0.102	0.007	−0.379	0.013	−0.494	0.006	−0.177	0.005
161.6	0.124	0.006	−0.443	0.013	−0.479	0.010	−0.155	0.005
164.8	0.138	0.008	−0.468	0.015			−0.127	0.006

x symbols. Generally, our new data at 186.6 MeV/N agree quite well with the data at 200 MeV/N for the analyzing powers iT_{11}, T_{20}, and T_{21}, while a rather large difference is found at the forward angles $\theta_{\mathrm{c.m.}} \lesssim 60^\circ$ for the tensor analyzing power T_{22}.

In the panels (e) of Figs. 1–4, the data sets are compared to the 190 MeV/N theoretical predictions based on the semiphenomenological standard NN potentials alone or in combination with the TM99 3NF. The (blue) dark shaded bands cover the predictions of AV18, CD Bonn, Nijmegen 1, and Nijmegen 2 potentials and the (red) light shaded bands cover the corresponding predictions when the TM99 3NF is included in the calculations. Also, the results for the AV18+Urbana IX combination are shown by (black) dashed curves. The (green) solid curves represent the predictions of the locally regularized N^{4}LO chiral potential with regulator $R = 0.9$ fm.

Comparing the standard NN and NN+3NF predictions, one finds that at 190 MeV/N quite large effects of the TM99 and Urbana IX 3NF's are visible for iT_{11}, T_{21}, and T_{22} while for T_{20} the predicted 3NF effects are rather small. These effects are localized in the region of the c.m. scattering angles $\theta_{\mathrm{c.m.}} \gtrsim 80^\circ$ where large 3NF effects are also predicted for the elastic scattering cross section [see Fig. 5(e)]. Generally the magnitudes of predicted 3NF effects for the TM99 and Urbana IX models are similar. The largest model dependence is seen in the tensor analyzing power T_{21} [see Fig. 3(e)]. Namely, for T_{21}, taking the AV18 NN potential and replacing TM99 by Urbana IX 3NF leads to quite different results at the angles $80^\circ \lesssim \theta_{\mathrm{c.m.}} \lesssim 160^\circ$. These features may come from the inconsistency of applied 2N and 3N forces which are derived independently using different theoretical approaches. This should be improved in the future by using consistent NN and 3N forces constructed in the framework of chiral EFT. We see that some of the predicted 3NF effects are supported by the data. For iT_{11}, the data roughly support the predicted effects both for the TM99 and the Urbana IX 3NF's. However, this is not the case for T_{21} and T_{22}. For T_{22}, the inclusion of the TM99 and the Urbana IX 3NF's improve the description of the data at angles $\theta_{\mathrm{c.m.}} \gtrsim 90^\circ$ while at smaller angles ($\theta_{\mathrm{c.m.}} \lesssim 80^\circ$) the data for T_{22} are closer to the calculations based on the pure NN potentials. For T_{21}, the smaller Urbana IX 3NF effects at angles $\theta_{\mathrm{c.m.}} \gtrsim 90^\circ$ are preferred by data in contrast to the larger effects of the TM99 3NF. For T_{20}, the theoretical predictions agree well with the data except for the backward angles $110^\circ \lesssim \theta_{\mathrm{c.m.}} \lesssim 150^\circ$, where the data are clearly underestimated by all the calculations, both without and with 3NFs.

Comparing results of calculations employing the chiral NN potential with those of the standard NN potentials, one finds that they provide similar results for T_{20} and T_{22} [see Figs. 2(e) and 4(e)]. These features are the same for the cross section [see Fig. 5(e)]. For the analyzing powers iT_{11} and T_{21} [see Figs. 1(e) and 3(e)], the results are significantly different at the

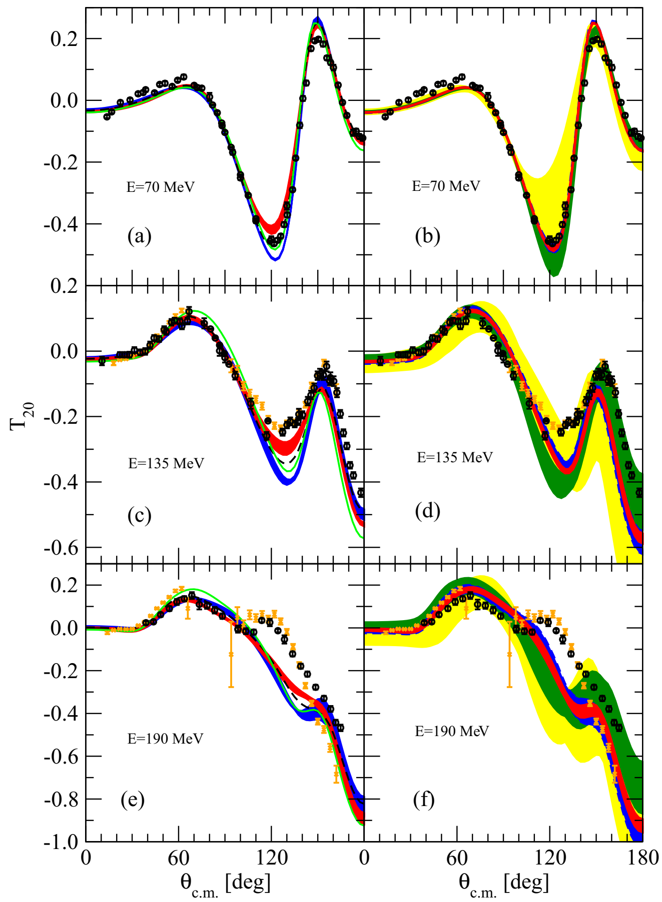

FIG. 2. The elastic Nd scattering tensor analyzing power T_{20} at the incoming nucleon laboratory energies $E = 70$ MeV [(a), (b)], 135 MeV [(c), (d)], and 190 MeV [(e), (f)]. See Fig. 1 for description of bands, curves, and data symbols.

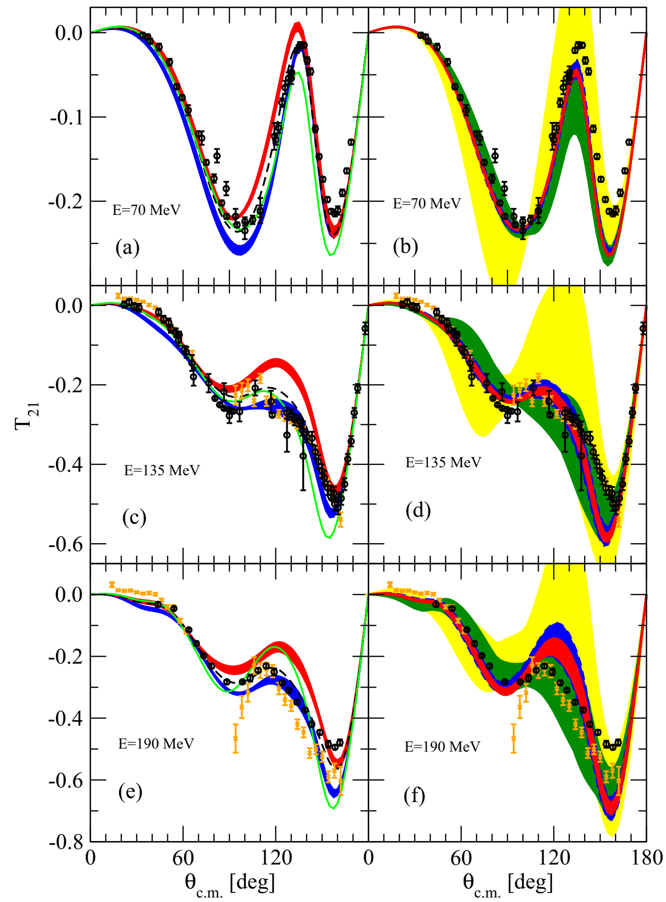

FIG. 3. The elastic Nd scattering tensor analyzing power T_{21} at the incoming nucleon laboratory energies $E = 70$ MeV [(a), (b)], 135 MeV [(c), (d)], and 190 MeV [(e), (f)]. See Fig. 1 for description of bands, curves, and data symbols.

angles around $\theta_{c.m.} = 110^\circ$, where the chiral predictions lie above semiphenomenological potential results, coming closer to the NN+TM99 predictions.

The complete set of all the deuteron analyzing powers was measured at RIKEN at incident energies from 70 up to 294 MeV/N, allowing us to investigate how the picture changes with energy. In the panels (a)–(d) of Figs. 1–4, we show the data and theoretical results at two other energies: 70 and 135 MeV/N. As for 135 MeV/N, the data from Ref. [26] are also presented, and they agree quite well with our data. At 70 MeV/N [Figs. 1(a), 2(a) 3(a), and 4(a)], where effects of a 3NF become visible in the elastic scattering cross section [Fig. 5(a)], only small 3NF effects are predicted for iT_{11} [Fig. 1(a)] and T_{20} [Fig. 2(a)]. All the theoretical predictions generally follow the experimental data. As for T_{21} [Fig. 3(a)] and T_{22} [Fig. 4(a)], moderate 3NF effects are seen and the data prefer the Urbana IX 3NF over the TM99 model. The 3NF effects become generally larger for the cross section and analyzing powers for the higher energy of 135 MeV/N [Figs. 1(c), 2(c), 3(c), 4(c), and 5(c)]. For iT_{11} and T_{20}, they are supported by the data both for the TM99 and Urbana IX 3NF's. For T_{21}, the data seem to favor again the Urbana IX 3NF. For T_{22}, the picture is unclear. Inclusion of the 3NF's shifts the predictions even further away from the data at scattering angles around $60^\circ \lesssim \theta_{c.m.} \lesssim 120^\circ$. Going to even larger energies than 190 MeV/N, namely 250 and 294 MeV/N, basically gives patterns similar to those obtained at 190 MeV/N [33]. It should be noted that at the two highest energies, large differences between the data and any theoretical calculations are more pronounced for almost all the observables at the very backward angles $\theta_{c.m.} \gtrsim 120^\circ$ [33]. We would also like to stress that the discrepancies between cross-section data and theory seen in Figs. 5(a)–5(d) for angles $\theta_{c.m.} \lesssim 30^\circ$ are due to pp Coulomb force [53], which is omitted in our calculations.

The N^{4}LO chiral potential predictions are close to semiphenomenological NN results at 70 and 135 MeV for the cross sections, iT_{11}, T_{20}, and T_{22}, but differ in the case of T_{21}. At higher energies, N^{4}LO NN predictions are generally different from the data. That would indicate effects of 3NF contributions, neglected in our calculations, which grow with the incident energy.

We estimated theoretical truncation uncertainties of our locally regularized chiral NN force predictions at different orders of chiral expansion using the procedure described in Ref. [52] and the scale parameter $\Lambda_b = 600$ MeV. The bands of different colors and decreasing width in the panels (b),

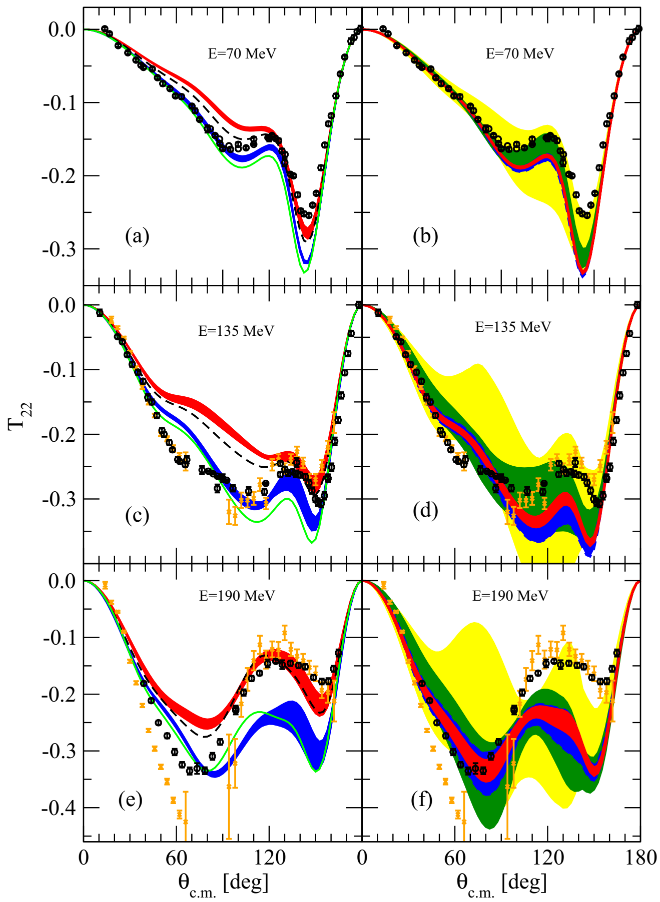

FIG. 4. The elastic Nd scattering tensor analyzing power T_{22} at the incoming nucleon laboratory energies $E = 70$ MeV [(a), (b)], 135 MeV [(c), (d)], and 190 MeV [(e), (f)]. See Fig. 1 for description of bands, curves, and data symbols.

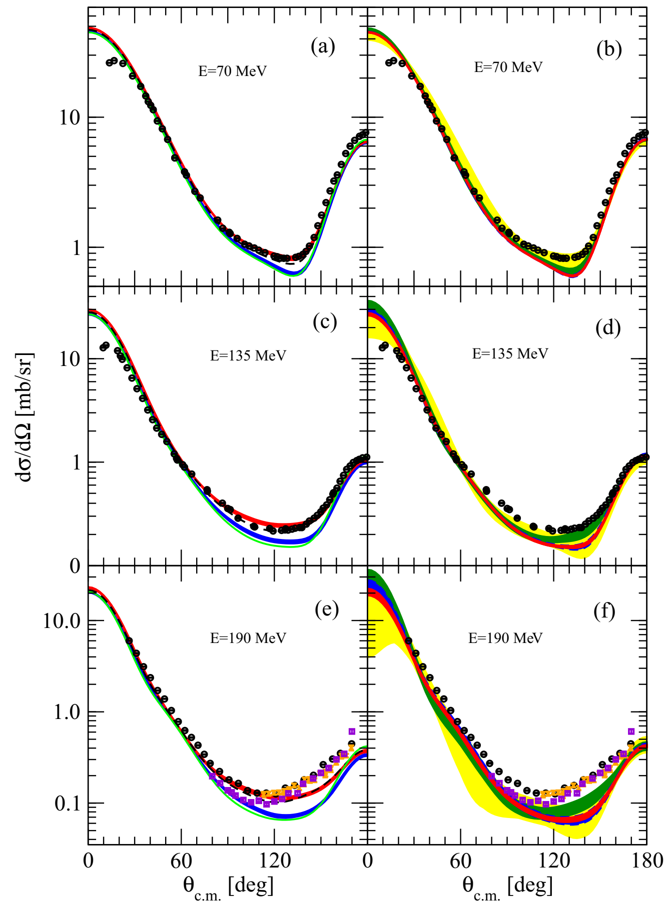

FIG. 5. The elastic Nd scattering cross section at the incoming nucleon laboratory energies $E = 70$ MeV [(a), (b)], 135 MeV [(c), (d)], and 190 MeV [(e), (f)]. The different symbols are dp or pd data: (black) circles in panels (a) and (b) from Ref. [18], in panels (c) and (d) from Refs. [13,16,18], and in panels (e) and (f) from Ref. [22]. In panels (e) and (f), the (orange) x symbols are from Ref. [54] and the (violet) squares are from Ref. [55]. See Fig. 1 for description of bands and curves.

(d), and (f) of Figs. 1–5 show these theoretical uncertainties, starting from NLO, through N^{2}LO, N^{3}LO, and N^{4}LO. It is clear that the width of estimated error band at N^{4}LO is the smallest for each observable and energy. That width grows with the increasing incident energy and its magnitude allows one to expect that N^{4}LO calculations can describe Nd scattering observables with sufficient accuracy up to energies of ≈200 MeV. One also finds that for N^{2}LO the truncation errors are of the order of the discrepancy between N^{4}LO predictions and the data. Since our chiral calculations neglect chiral 3NF's, which for the first time appear at N^{2}LO, one can expect that those discrepancies can be probably explained when omitted chiral 3NF's are included in future calculations.

V. SUMMARY AND CONCLUSIONS

We have reported a complete set of high-precision data for the deuteron analyzing powers iT_{11}, T_{20}, T_{21}, and T_{22}, in elastic dp scattering at 186.6 MeV/nucleon, taken in a wide angular range $39^\circ \leqslant \theta_{\rm c.m.} \leqslant 165^\circ$. For all the deuteron analyzing powers, the statistical uncertainties are smaller than 0.02 and the systematic uncertainties do not exceed the statistical ones. These data, together with our previously reported deuteron analyzing powers taken at different energies, constitute a solid basis to guide theoretical investigations of 3NFs.

Our new deuteron analyzing powers and the previously measured data at 70 and 135 MeV/nucleon, together with the elastic cross-section data in the energy region of interest, are compared with the results of 3N Faddeev calculations based on the standard NN potentials alone or combined with the TM99 3NF. The AV18 NN potential is also combined with the Urbana IX 3NF.

Clear discrepancies between theory restricted to the standard NN potentials and the data have been found at the angles $\theta_{\rm c.m.} \gtrsim 80^\circ$, especially for the deuteron analyzing powers iT_{11} and T_{22} as well as for the differential cross section. The observed discrepancies indicate large 3NF effects for these observables. The predicted 3NF effects grow with the increasing incident energy. The TM99 and the Urbana IX 3NFs give similar effects for almost all the studied observables except for the tensor analyzing power T_{21}, where the stronger dependence on the 3*N*F model has been found. However, the experimental data are not always explained by the calculations with the 3*N*Fs, confirming the complex pattern of the 3*N*F effects in spin observables. These results indicate that one needs additional components of 3*N*Fs other than those of 2π-exchange nature. The observed model dependence of the spin observables calls for using consistent 2*N* and 3*N* forces in a theoretical analysis.

In order to see how the chiral *NN* forces describe the elastic *Nd* scattering, the calculations based on the locally regularized N^4LO *NN* potential are shown and compared with the data. Generally, the presented calculations based on the chiral N^4LO *NN* potential yield similar predictions to the standard *NN* potentials for the cross section as well as for the deuteron analyzing powers. However, at higher energies, the chiral N^4LO results differ significantly from other predictions for iT_{11}, T_{21}, and T_{22}. Estimated theoretical truncation errors at different orders of chiral expansion decrease rapidly with the increasing order, which allows us to conclude that N^4LO chiral calculations posses sufficient precision to describe *Nd* scattering observables. The deviation of such predictions from the data has the same order of magnitude as the theoretical uncertainty of chiral calculations at N^2LO. Since at that order a 3*N*F appears for the first time, it supports additionally the conclusion that the discrepancies between pure pairwise theory and the data found by us probably could be explained by including chiral 3*N*F's in our calculations. That conclusion must be verified in future calculations, when consistent 2*N* and 3*N* forces up to at least N^3LO are applied.

ACKNOWLEDGMENTS

This experiment was performed at RI Beam Factory operated by RIKEN Nishina Center and CNS, University of Tokyo. This work was supported financially in part by the Grants-in-Aid for Scientific Research No. 20684010, No. 24684013, and No. 16H02171 of the Ministry of Education, Culture, Sports, Science, and Technology of Japan. It was also partially supported by the Polish National Science Center under Grants No. DEC2013/10/M/ST2/00420 and No. 2016/22/M/ST2/00173 and by the Japan Society for Promotion of Science (JSPS ID No. S-16020). The numerical calculations were performed on the supercomputer cluster of the JSC, Jülich, Germany.

[1] W. Glöckle, H. Witała, D. Hüber, H. Kamada, and J. Golak, Phys. Rep. **274**, 107 (1996).
[2] H.-W. Hammer, A. Nogga, and A. Schwenk, Rev. Mod. Phys. **85**, 197 (2013), and references therein.
[3] N. Kalantar-Nayestanaki, E. Epelbaum, J. G. Messchendorp, and A Nogga, Rep. Prog. Phys. **75**, 016301 (2012).
[4] R. B. Wiringa, V. G. J. Stoks, and R. Schiavilla, Phys. Rev. C **51**, 38 (1995).
[5] R. Machleidt, Phys. Rev. C **63**, 024001 (2001).
[6] V. G. J. Stoks, R. A. M. Klomp, C. P. F. Terheggen, and J. J. de Swart, Phys. Rev. C **49**, 2950 (1994).
[7] S. A. Coon and H. K. Han, Few-Body Syst. **30**, 131 (2001).
[8] B. S. Pudliner, V. R. Pandharipande, J. Carlson, S. C. Pieper, and R. B. Wiringa, Phys. Rev. C **56**, 1720 (1997).
[9] H. Witała, W. Glöckle, D. Huber, J. Golak, and H. Kamada, Phys. Rev. Lett. **81**, 1183 (1998).
[10] W. P. Abfalterer, F. B. Bateman, F. S. Dietrich, C. Elster, R. W. Finlay, W. Glöckle, J. Golak, R. C. Haight, D. Huber, G. L. Morgan, and H. Witala, Phys. Rev. Lett. **81**, 57 (1998).
[11] H. Witała, H. Kamada, A. Nogga, W. Glöckle, Ch. Elster, and D. Hüber, Phys. Rev. C **59**, 3035 (1999).
[12] H. Witała, W. Glöckle, J. Golak, A. Nogga, H. Kamada, R. Skibiński, and J. Kuroś-Żołnierczuk, Phys. Rev. C **63**, 024007 (2001).
[13] N. Sakamoto *et al.*, Phys. Lett. B **367**, 60 (1996).
[14] E. J. Stephenson, H. Witała, W. Glöckle, H. Kamada, and A. Nogga, Phys. Rev. C **60**, 061001(R) (1999).
[15] R. Bieber, W. Glöckle, J. Golak, M. N. Harakeh, D. Hüber, H. Huisman, N. Kalantar-Nayestanaki, H. Kamada, J. G. Messchendorp, A. Nogga, H. Sakai, N. Sakamoto, M. Seip, M. Volkerts, S. Y. van der Werf, and H. Witała, Phys. Rev. Lett. **84**, 606 (2000).
[16] H. Sakai, K. Sekiguchi, H. Witała, W. Glöckle, M. Hatano, H. Kamada, H. Kato, Y. Maeda, A. Nogga, T. Ohnishi *et al.*, Phys. Rev. Lett. **84**, 5288 (2000).
[17] K. Ermisch, A. M. van den Berg, R. Bieber, W. Glöckle, J. Golak, M. Hagemann, V. M. Hannen, M. N. Harakeh, M. A. de Huu, N. Kalantar-Nayestanaki, H. Kamada *et al.*, Phys. Rev. Lett. **86**, 5862 (2001).
[18] K. Sekiguchi, H. Sakai, H. Witała, W. Glöckle, J. Golak, M. Hatano, H. Kamada, H. Kato, Y. Maeda, J. Nishikawa *et al.*, Phys. Rev. C **65**, 034003 (2002).
[19] K. Hatanaka, Y. Shimizu, D. Hirooka, J. Kamiya, Y. Kitamura, Y. Maeda, T. Noro, E. Obayashi, K. Sagara, T. Saito *et al.*, Phys. Rev. C **66**, 044002 (2002).
[20] K. Sekiguchi, H. Sakai, H. Witała, K. Ermisch, W. Glöckle, J. Golak, M. Hatano, H. Kamada, N. Kalantar-Nayestanaki, H. Kato *et al.*, Phys. Rev. C **70**, 014001 (2004).
[21] H. O. Meyer, T. J. Whitaker, R. E. Pollock, B. von Przewoski, T. Rinckel, J. Doskow, J. Kuroś-Żołnierczuk, P. Thörngren-Engblom, P. V. Pancella, T. Wise *et al.*, Phys. Rev. Lett. **93**, 112502 (2004).
[22] K. Ermisch, H. R. Amir-Ahmadi, A. M. van den Berg, R. Castelijns, B. Davids, A. Deltuva, E. Epelbaum, W. Glöckle, J. Golak, M. N. Harakeh *et al.*, Phys. Rev. C **71**, 064004 (2005).
[23] K. Sekiguchi, H. Sakai, H. Witała, W. Glöckle, J. Golak, K. Hatanaka, M. Hatano, K. Itoh, H. Kamada, H. Kuboki *et al.*, Phys. Rev. Lett. **95**, 0162301 (2005).
[24] S. Kistryn, E. Stephan, A. Biegun, K. Bodek, A. Deltuva, E. Epelbaum, K. Ermisch, W. Glöckle, J. Golak, N. Kalantar-Nayestanaki *et al.*, Phys. Rev. C **72**, 044006 (2005).
[25] P. Mermod, J. Blomgren, C. Johansson, A. Öhrn, M. Österlund, S. Pomp, B. Bergenwall, J. Klug, L. Nilsson, N. Olsson *et al.*, Phys. Rev. C **74**, 054002 (2006).
[26] B. v. Przewoski, H. O. Meyer, J. T. Balewski, W. W. Daehnick, J. Doskow, W. Haeberli, R. Ibald, B. Lorentz, R. E. Pollock, P. V. Pancella *et al.*, Phys. Rev. C **74**, 064003 (2006).
[27] Y. Maeda, T. Kawabata, K. Suda, H. Sakai, K. Fujita, K. Hatanaka, H. Okamura, Y. Sakemi, Y. Shimizu, Y. Tameshige *et al.*, Phys. Rev. C **76**, 014004 (2007).

[28] H. R. Amir-Ahmadi, R. Castelijns, A. Deltuva, M. Eslami-Kalantari, E. D. van Garderen, M. N. Harakeh, N. Kalantar-Nayestanaki, M. Kiš, H. Löhner, M. Mahjour-Shafiei *et al.*, Phys. Rev. C **75**, 041001 (2007).
[29] A. Ramazani-Moghaddam-Arani, H. R. Amir-Ahmadi, A. D. Bacher, C. D. Bailey, A. Biegun, M. Eslami-Kalantari, I. Gašspari, L. Joulaeizadeh, N. Kalantar-Nayestanaki, St. Kistryn *et al.*, Phys. Rev. C **78**, 014006 (2008).
[30] K. Sekiguchi, H. Sakai, H. Witała, W. Glöckle, J. Golak, K. Itoh, H. Kamada, T. Kawabata, H. Kuboki, Y. Maeda *et al.*, Phys. Rev. C **79**, 054008 (2009).
[31] H. Mardanpour, H. R. Amir-Ahmadi, R. Benard, A. Biegun, M. Eslami-Kalantari, L. Joulaeizadeh, N. Kalantar-Nayestanaki, M. Kiš, St. Kistryn, A. Kozela *et al.*, Phys. Lett. B **687**, 149 (2010).
[32] K. Sagara, Few-Body Syst. **48**, 59 (2010).
[33] K. Sekiguchi, Y. Wada, J. Miyazaki, H. Witała, M. Dozono, U. Gebauer, J. Golak, H. Kamada, S. Kawase, Y. Kubota *et al.*, Phys. Rev. C **89**, 064007 (2014).
[34] H. Witała, J. Golak, W. Glöckle, and H. Kamada, Phys. Rev. C **71**, 054001 (2005).
[35] H. Witała, J. Golak, R. Skibiński, W. Glöckle, W. N. Polyzou, and H. Kamada, Phys. Rev. C **77**, 034004 (2008).
[36] E. Epelbaum, Prog. Part. Nucl. Phys. **57**, 654 (2006).
[37] R. Machleidt and D. R. Entem, Phys. Rep. **503**, 1 (2011).
[38] E. Epelbaum, A. Nogga, W. Glöckle, H. Kamada, U.-G. Meißner, and H. Witała, Phys. Rev. C **66**, 064001 (2002).
[39] V. Bernard, E. Epelbaum, H. Krebs, and U.-G. Meißner, Phys. Rev. C **77**, 064004 (2008).
[40] V. Bernard, E. Epelbaum, H. Krebs, and U.-G. Meißner, Phys. Rev. C **84**, 054001 (2011).
[41] E. Epelbaum, H. Krebs, and U.-G. Meißner, Eur. Phys. J. A **51**, 53 (2015).
[42] E. Epelbaum, H. Krebs, and U.-G. Meißner, Phys. Rev. Lett. **115**, 122301 (2015).
[43] K. Sekiguchi, H. Okamura, N. Sakamoto, H. Suzuki, M. Dozono, Y. Maeda, T. Saito, S. Sakaguchi, H. Sakai, M. Sasano *et al.*, Phys. Rev. C **83**, 061001(R) (2011).
[44] H. Okamura, H. Sakai, N. Sakamoto, T. Uesaka, S. Ishida, H. Otsu, T. Wakasa, K. Hatanaka, T. Kubo, N. Inabe *et al.*, *Polarized Ion Sources and Polarized Gas Targets*, AIP Conf. Proc. Vol. 293, edited by H. P. gen. Schieck and L. Sydow (AIP, New York, 1994), p. 84.
[45] T. Kubo, D. Kameda, H. Suzuki, N. Fukuda, H. Takeda, Y. Yanagisawa, M. Ohtake, K. Kusaka, K. Yoshida, N. Inabe *et al.*, Prog. Theor. Exp. Phys. **2012**, 03C003 (2012).
[46] K. Suda, H. Okamura, T. Uesaka, J. Nishikawa, H. Kumasaka, R. Suzuki, H. Sakai, A. Tamii, T. Ohnishi, K. Sekiguchi *et al.*, Nucl. Instrum. Methods Phys. Res. A **572**, 745 (2007).
[47] H. Okamura, N. Sakamoto, T. Uesaka, H. Sakai, K. Hatanaka, A. Goto, M. Kase, N. Inabe, and Y. Yano, *The 11Th International Symposium on High Energy Spin Physics*, AIP Conf. Proc. Vol. 343, edited by K. J. Heller and S. L. Smith (AIP, New York, 1995), p. 123.
[48] H. Witała, T. Cornelius, and W. Glöckle, Few-Body Syst. **3**, 123 (1988).
[49] D. Hüber, H. Kamada, H. Witała, and W. Glöckle, Acta Phys. Pol. B **28**, 1677 (1997).
[50] W. Glöckle, *The Quantum Mechanical Few-Body Problem* (Springer-Verlag, Berlin, 1983).
[51] H. Witała, J. Golak, R. Skibiński, and K. Topolnicki, J. Phys. G: Nucl. Part. Phys. **41**, 094011 (2014).
[52] S. Binder, A. Calci, E. Epelbaum, R. J. Furnstahl, J. Golak, K. Hebeler, H. Kamada, H. Krebs, J. Langhammer, S. Liebig *et al.*, Phys. Rev. C **93**, 044002 (2016).
[53] A. Deltuva, A. C. Fonseca, and P. U. Sauer, Phys. Rev. C **72**, 054004 (2005).
[54] G. Igo, J. C. Fong, S. L. Verbeck, M. Goitein, D. L. Hendrie, J. C. Carroll, B. McDonald, A. Stetz, and M. C. Makino, Nucl. Phys. A **195**, 33 (1972).
[55] R. E. Adelberger and C. N. Brown, Phys. Rev. D **5**, 2139 (1972).